



## Optimizing the micropore-to-mesopore ratio of carbon-fiber-cloth creates record-high specific capacitance

Ying Zheng<sup>a</sup>, Ting Deng<sup>a</sup>, Wei Zhang<sup>a,b,c,\*</sup>, Weitao Zheng<sup>a,\*\*</sup>

<sup>a</sup> State Key Laboratory of Automotive Simulation and Control, and School of Materials Science & Engineering, Electron Microscopy Center, and International Center of Future Science, Jilin University, Changchun 130012, Jilin, China

<sup>b</sup> Wuhan National Laboratory for Optoelectronics, Huazhong University of Science and Technology, Wuhan 430074, Hubei, China

<sup>c</sup> IKERBASQUE, Basque Foundation for Science, Bilbao 48013, Spain

### ARTICLE INFO

#### Article history:

Received 9 October 2019

Revised 19 November 2019

Accepted 15 December 2019

Available online 30 December 2019

#### Keywords:

Pore distribution

Hierarchical pores integration

Supercapacitors

Carbon fiber cloth

Electrochemical performance

### ABSTRACT

The application of commercial carbon fiber cloth (CFC) in energy storage equipment is limited by its low specific capacitance and energy density. By a simple one-step activation treatment, the specific surface area of CFCs with porous structure can be increased considerably from 3.9 up to 875 m<sup>2</sup>/g and the electrochemical properties of CFCs can be improved by three orders of magnitude (1324 mF/cm<sup>2</sup>). Moreover, the hydrophobicity of CFCs can be transformed into superhydrophilicity. However, the electrochemical performance of CFCs does not show a positive correlation with specific surface area but have a strong relationship with the hierarchical pore distribution forged by the annealing treatment. Only moderate micropore and mesoporous ratio enables optimizing the electrochemical performance of CFCs.

© 2019 Science Press and Dalian Institute of Chemical Physics, Chinese Academy of Sciences. Published by Elsevier B.V. and Science Press. All rights reserved.

### 1. Introduction

Carbon fiber cloth (CFC), ascribed to its advantages of excellent electrical conductivity, mechanical toughness, non-toxicity and mass-production [1–4], is promising for energy storage devices, such as electric double layer capacitors (EDLCs). CFC remains in its fancy, however, for practical application because of its very limited specific capacity and energy density. EDLC is originated from the electric double layer between electrode and electrolyte, in the form of both inner and outer surfaces of active materials [5–7]. Thus, expanding the specific surface area (SSA) of CFCs may be constructive to boost the specific capacitance and address the low energy density issues [8–14]. Nevertheless, no clear correlation between the specific capacitance and SSA has been found and the capacitance enhancement is still challenging [9]. Theoretically, creating abundant pore structures is expected to effectively afford desirable electrode structure, within which more electrolyte ions are stored. Therefore, a high-porosity and large surface area of CFCs enables

optimizing EDLC, provided if the effect of pore size and structure can be well resolved on capacitance.

For instance, within the pore size less than the double-sized solvated ions, a capacitance was found to increase rapidly with the decrease of pore size [15]. This breaks the traditional notion that the presence of ultra-micropores cannot contribute to capacitance. By using the quartz crystal microbalance, it was confirmed that hydrated ions can enter into the ultra-micropores [16]. On the other hand, an appropriate ratio of micropores to mesopores is conducive to the improvement of ordered mesoporous carbons CMK-3 capacitance [17]. Nevertheless, such findings simply link pore sizes and volumes. How to architect the hierarchical macropore/micropore/mesopore volumes in CFCs and explore the intrinsic correlation on electrochemical performance has been rarely reported.

A synergistic effect of hierarchical pores is crucial to the performance of electrode. Macropores can be regarded as ion storage reservoirs which shorten ion diffusion distances towards interior materials after immersed in the electrolyte. Mesopore structures are the critical composition that influences electrolyte accessibility and ion transportation, leading ultimately to the electrochemical performances. Micropores (<1–2 nm) can afford an ultrahigh capacitance [17–20]. Since different levels of pores have various effects on the overall performance of material, it is crucial

\* Corresponding author at: State Key Laboratory of Automotive Simulation and Control, and School of Materials Science & Engineering, Electron Microscopy Center, and International Center of Future Science, Jilin University, Changchun 130012, Jilin, China.

\*\* Corresponding author.

E-mail addresses: [weizhang@jlu.edu.cn](mailto:weizhang@jlu.edu.cn) (W. Zhang), [\(W. Zheng\).](mailto:wtzheng@jlu.edu.cn)

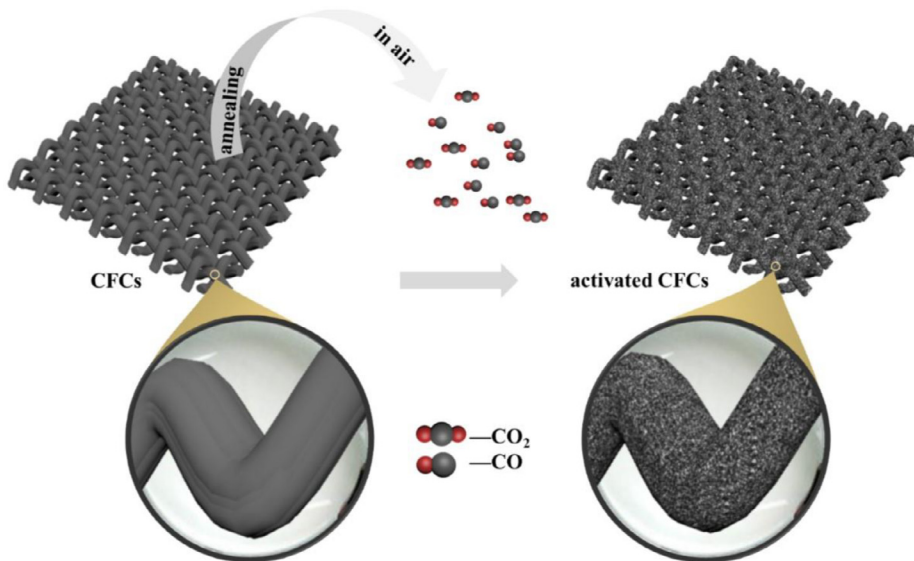


**Fig. 1.** Schematic illustration of the preparation process of activated carbon fiber cloths.

to study the relationship between the overall proportion of macropores, mesopores and micropores.

Herein, we simply anneal a commercial carbon fiber cloth as the active material. Our route not only effectively increased the specific surface area of CFCs from 3.9 up to  $875\text{ m}^2/\text{g}$ , but also harvested the structure integrating different hierarchical pores in correlation with various annealing temperatures. Mechanistic insight into the proportion of different micropores, mesopores and larger pores on the capacitance performance was gained for the activated CFCs.

## 2. Experimental

### 2.1. Active carbon cloth preparation

Commercial carbon fiber cloths tailored as  $1 \times 1.5\text{ cm}^2$  were applied with the impurity eliminated on the surface, in a solution of acetone, alcohol and deionized water solution respectively under ultra-sound conditions for 20 min. And then it was put into a drying oven at  $60^\circ\text{C}$  overnight. Annealed in the muffle furnace (SXL-1400C, Shanghai Jyjing Precision Instrument Manufacturing Co., LTD) under ambient condition, the temperature was set as 350, 400, 425, 450, 475 °C with a rate of  $5^\circ\text{C}/\text{min}$  and the duration of 2 h. The furnace of SXL-1400C is equipped with breathing holes and air outlet, which facilitates gas exchange. The constant pressure can be maintained. Finally, we obtained the activated carbon fiber cloth labeled as 350CFC, 400CFC, 425CFC, 450CFC and 475CFC.

### 2.2. Material characterization

Power X-ray diffraction (XRD) analysis was performed on a Bruker D8 Advance diffract meter with a Cu  $K_\alpha$  radiation ( $\lambda = 0.15418\text{ nm}$ ). Scanning electron microscopy (SEM, Hitachi SU8010) was used to characterize the morphology. X-ray photoelectron spectroscopy (XPS, ESCLAB-250) analysis was performed with a monochromatic Al  $K_\alpha$  radiation source and a hemisphere detector with an energy resolution of 0.1 eV. (ASAP 2020 PLUS HD88). The pore structure and specific area were measured by using Silica alumina ISO N2@77 K. Raman analysis was conducted by a TESCAN RISE (MIRA3) instrument. Contact angle measurements was made by Krüss DSA 30.

### 2.3. Electrochemical test

Cyclic voltammogram (CV) test was conducted using CHI660E electrochemical workstation (Shanghai CH Instrument Company, China). The electrochemical impedance spectroscopy (EIS) of electrodes was measured by using a PARATAT 2273 advanced electrochemical system. Single electrode was measured in a conventional three-electrode cell with a platinum plate counter and SCE reference electrodes. 1 M KOH aqueous solution was used as the electrolyte. All the electrochemical characterization and analysis were recorded at room temperature.

## 3. Results and discussion

Activated carbon fiber cloths (ACFCs) with different hierarchical pores were obtained by annealing at different temperatures. The experimental process is described in Fig. 1. The activated carbon fiber cloths are characterized and analyzed. XRD pattern (Fig. S1) proved that the phase composition of ACFCs remained even after high-temperature annealing. However, judged from SEM observations the morphology of the ACFCs has been significantly modified. As shown in Fig. 2(a), the carbon fibers can be observed for the pristine sample. Each carbon fiber is covered by amounts of thin carbon slices. The carbon fiber surface beneath thin slices is smooth as revealed from the inset. After the annealing, obvious changes have occurred on the surface of carbon fibers. Fig. 2(b-f) is the typical SEM images of 350CFC, 400CFC, 425CFC, 450CFC and 475CFC, respectively. One can clearly find that the thin slices disappeared gradually with the escalation of annealing temperatures until completely vanished at  $475^\circ\text{C}$ . Besides, the surface of carbon fibers has been also changed roughly. Hierarchical pores were observed, due to the formation/escaping of CO and  $\text{CO}_2$  molecules in the high-temperature treatment [21].

Raman imaging and secondary electron microscopy (RISE) were used for further structural characterization. The Raman and SEM images were superimposed according to different mixing degrees to obtain the RISE images, as shown in Fig. 2(g-l). The disordered degree of the material surface can be obtained by analyzing the intensity ratio of peaks G and D, where they represent graphite band ( $\sim 1582\text{ cm}^{-1}$ ) and disorder-induced band ( $\sim 1350\text{ cm}^{-1}$ ), respectively [22]. In Fig. 2(g-l), the red, blue, green, purple and yellow areas represent the high-G/D, middle-G/D, low-G/D, background and

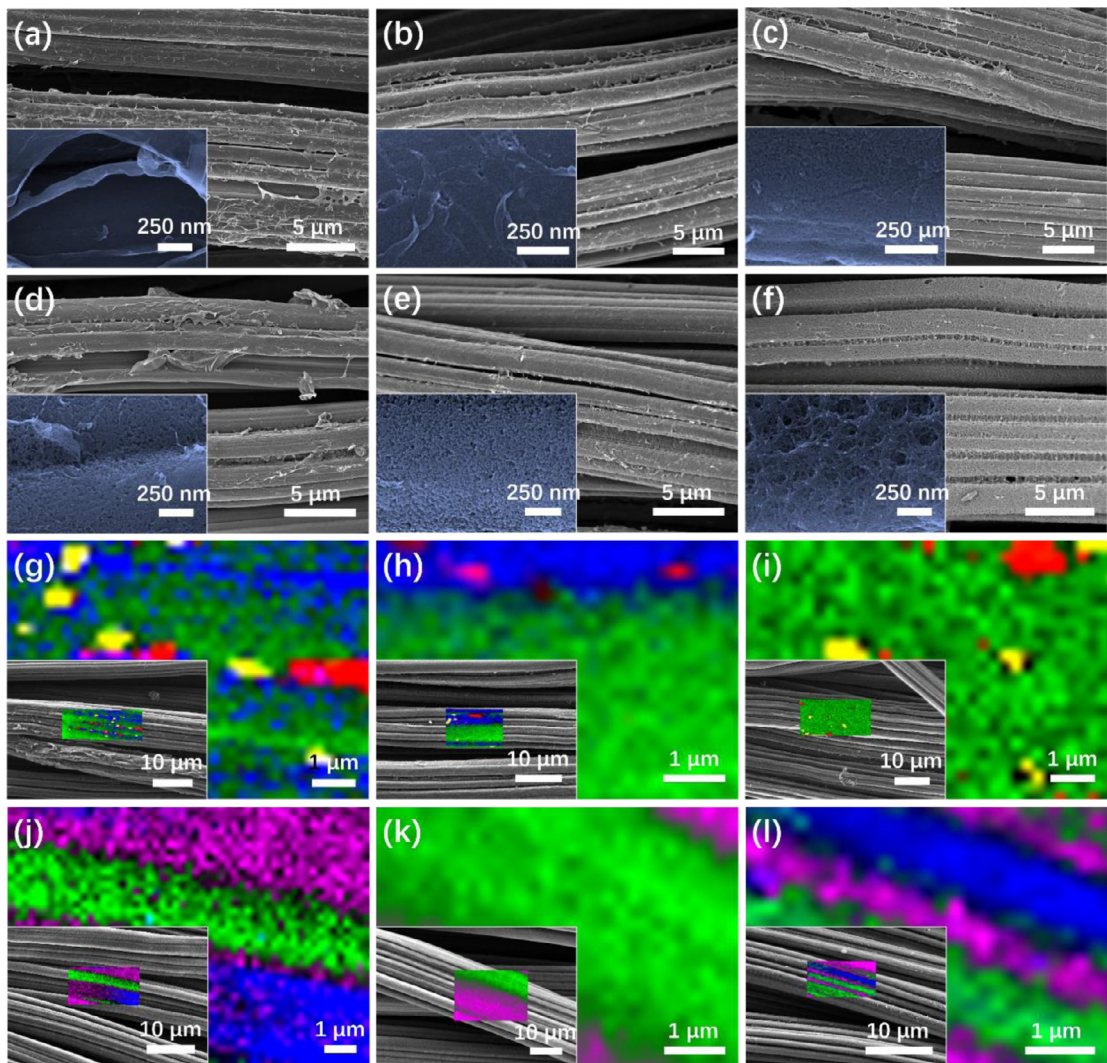


**Fig. 2.** Morphological and Raman analysis. SEM images of (a) CFC, (b–f) CFC calcined at various temperatures of 350, 400, 425, 450 and 475 °C. (g–l) RISE images of CFC, 350CFC, 400CFC, 425CFC, 450CFC and 475CFC, respectively. The insets are the corresponding SEM images with local RISE information.

fluorescent regions, respectively. There are fewer red regions and more green regions in the original CFC, 350CFC and 400CFC. The overall distribution tends to be more disordered, confirming the existence of amorphous carbon and edge defects on the surface [23]. Compared with Fig. 2(j–l) and 2(g–i), there is no red region but more blue region in 425CFC, 450CFC and 475CFC, indicating that annealing increases the disorder degree of CFCs. There is no high G/D region when the temperature exceeds 400 °C. It is worth noting that neither red nor blue regions appear in the 450CFC, which consists mainly of green regions. This indicates that 450CFC has a higher disorder degree with a relatively uniform distribution.

The surface states of carbon fibers are analyzed through X-ray photoelectron spectroscopy (XPS). The XPS spectra of CFC, 425CFC, 450CFC and 475CFC are further analyzed. Fig. 3(a) represents the evolution of C1s at different temperatures, ascribed to C–C, C–O and O–C=O at 284.8, 285.9 and 289.3 eV, respectively [24,25]. C–C decreased gradually with the temperature increase. Both C–O and O–C=O increase after the annealing. Fig. 3(b) shows O1s containing three peaks, C=O (532.5), C–O (533.5) and O–C=O (535.5 eV), respectively [26,27]. Both C–O and O–C=O also increase after the annealing, as Table S1, which is consistent with the result of C1s. C–O, C=O and O–C=O are hydrophilic groups. The increase of hydrophilic surface groups is conducive to the material hydrophilicity,

enabling to improve contact with the electrolyte. Further, the contact angle measurements confirm that the hydrophilicity of the annealed CFC increased significantly. One can find in the original CFC a contact angle above 90°, i.e., hydrophobic (Gif S1a). However, for the annealed 450CFC, the droplet will be completely and immediately soaked when it comes into contact with the surface (Gif S1b). That is to say, 450CFC is super-hydrophilic. All these evidences prove that the annealing process changes the CFCs from hydrophobic to hydrophilic. Thus, the ACFCs can optimize contact with the electrolyte.

The BET surface area characterized by using nitrogen adsorption/desorption experiments as shown in Figs. 4(d) and S2, considering that obvious pores were observed from the SEM images. The original CFC has a Type-V adsorption–desorption isotherm which proves the presence of mesoporous pores [8]. The BET surface area of the original CFC is 3.9 m<sup>2</sup>/g, probably due to the surface carbon slices. 350CFC, 400CFC, 425CFC, 450CFC and 475CFC show a Type-I adsorption–desorption isotherms. It is characteristic of the rapid increase of adsorption quantity when the relative pressure is low. It reflects the micropore adsorption [28]. Once the relative pressure was 0.4–0.8 Pa, the appearance of H4 type hysteresis ring demonstrates the existence of slit holes. The specific surface areas are 114, 434, 459, 614 and 875 m<sup>2</sup>/g, respectively. Thus, the an-

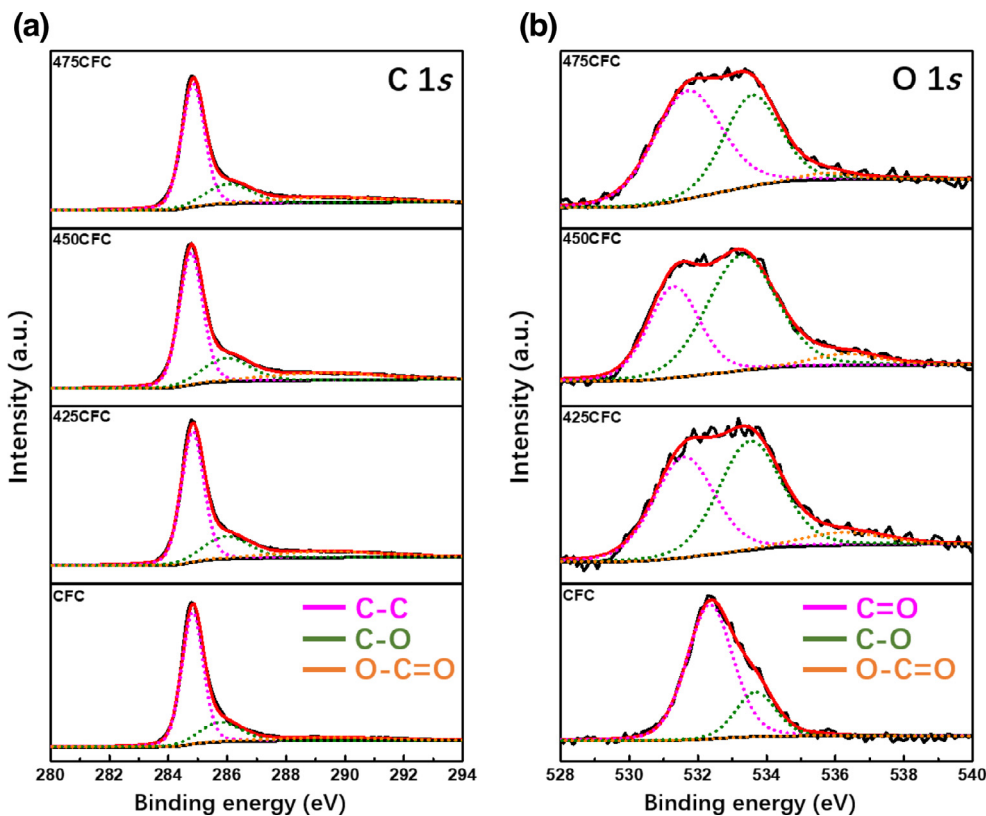


**Fig. 3.** Surface state analysis of samples. (a) C 1s and (b) O 1s XPS spectra of CFC, 425CFC, 450CFC and 475CFC.

nealing process significantly increased the specific surface area of CFCs.

Electrochemical tests were carried out in order to explore the electrochemical properties of ACFCs. Fig. 4(a) shows the cyclic voltammetry curves of CFC, 425CFC, 450CFC and 475CFC at the sweep rate of 5 mV/s. There is no capacity in the potential range of -1–0 V as CFC has a low specific surface area. This is also the reason that commercial carbon cloth is generally used as a substrate rather than directly used as electrode active material. For 425CFC, 450CFC and 475CFC all show rectangular peaks, consistent with a typical double-layer behavior. Under the current density of 2 mA/cm<sup>2</sup>, ACFCs were charged and discharged. The capacitance of 425CFC, 450CFC and 475CFC are 940 (85 F/g), 1324 (146 F/g) and 1020 (183 F/g) mF/cm<sup>2</sup>, respectively, as shown in Fig. 4(b). The capacitances of 350CFC and 400CFC are 242 and 944 mF/cm<sup>2</sup>, respectively. Their rectangular peaks are shown in Fig. S3(a, b). The 450CFC has a maximum specific capacity of 1324 mF/cm<sup>2</sup>, comparable to what has been achieved by electrochemical, chemical and heterogeneous atom recombination methods to activate carbon materials, as shown in Table 1. Interestingly, no capacitance increase occurred with the increase of the specific surface area. This may be correlated to their hierarchical pore integration, conforming to the porosity distribution analysis by Original Density Functional Theory. From Fig. S4(a), one can see that the total pore volume ( $V_t$ ) of the original CFC is 0.12 cm<sup>3</sup>/g, while that of 350CFC, 400CFC, 425CFC, 450CFC and 475CFC are 0.5, 0.17, 0.20, 0.28 and 0.38 cm<sup>3</sup>/g, respectively. That leads to a gradual increase in the specific surface area. The pore size distribution was shown in Fig. 4(e). There are mesopores in the original CFC with no hierarchical porous structure; the pore width was concentrated at ~5 nm. A hierarchical porous structure occurred in the 425CFC, 450CFC and 475CFC samples; the micropore widths are mainly 0.68–1.27 nm. Obviously, it is the existence of hierar-

chical porous to increase the capacity of CFC. Hierarchical porous also exists in 350CFC and 400CFC, as shown in Fig. S4(c). SAIEUS software (downloaded at [www.nldft.com](http://www.nldft.com)) was used to calculate the adsorption and desorption data by line fitting in order to obtain more detailed pores distribution information. The Carbon-N2-2DNLDTF Heterogeneous Surface model was selected for this calculation. This method has been widely used to analyze pore size distribution [29,30]. The results are shown in Figs. 4(f) and S4(d). The content of micropore and mesopore increased gradually with the increase of annealing temperature, and more ultra-micropore existed in 450CFC. More specific pore volume analysis is shown in Table 2. The volume of macropore ( $V_{mac}$ ) and the ratio of the volume of macropore to the total pores ( $V_{mac}/V_t$ ) are very small in the five samples. Macropores can shorten the diffusion distance of ions and reduce the resistance of ion diffusion because the physicochemical properties of electrolyte ions in macropores are similar to those of electrolyte ions in solution so the macropores can improve the rate capability [19]. However, the pore depth of micropores and mesopores also affect the rate capability of active materials. For mesopores, the volume of mesopore ( $V_{mes}$ ) and the ratio of the volume of mesopore to the total pores ( $V_{mes}/V_t$ ) increase gradually with the increase of annealing temperature when the temperature exceeds 350 °C. Mesopores can increase the electron/ion transfer rate and afford a double layer to increase the specific capacitance. For micropores, the volume of micropore ( $V_{mic}$ ) gradually increases. Whereas the ratio of the volume of micropore to the total pores ( $V_{mic}/V_t$ ) is reversed in 400CFC, 425CFC, 450CFC and 475CFC. The results showed that  $V_{mic}/V_{mes}$  became smaller with the increase of annealing temperature when the temperature exceeds 350 °C. The presence of micropores can significantly improve the material capacity, as the hydrated ions strip off the hydrated shells [16,31] or the hydrated shell deforms [15,32] into the micropores. The smaller space in micropores effectively reduces the dis-

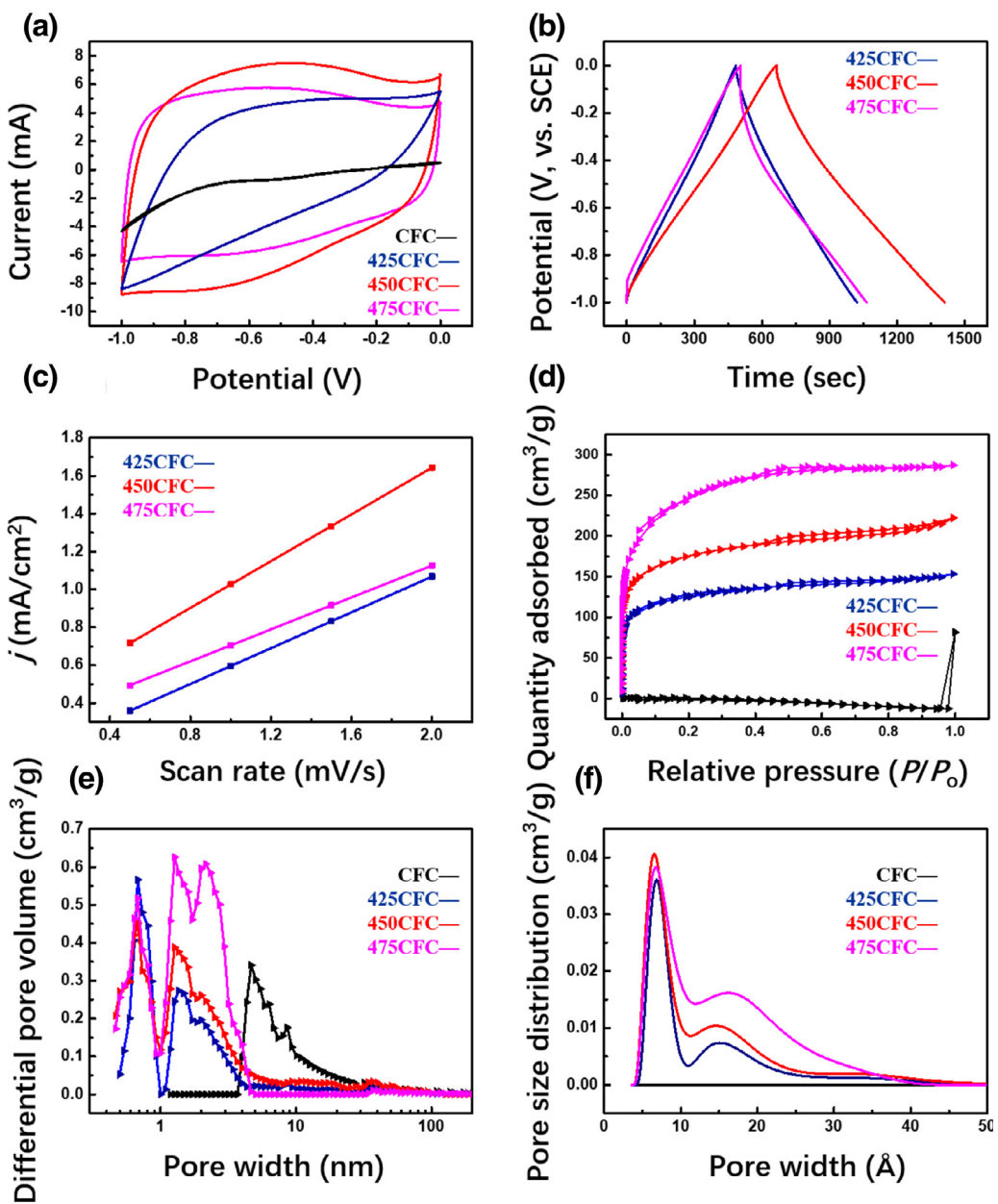


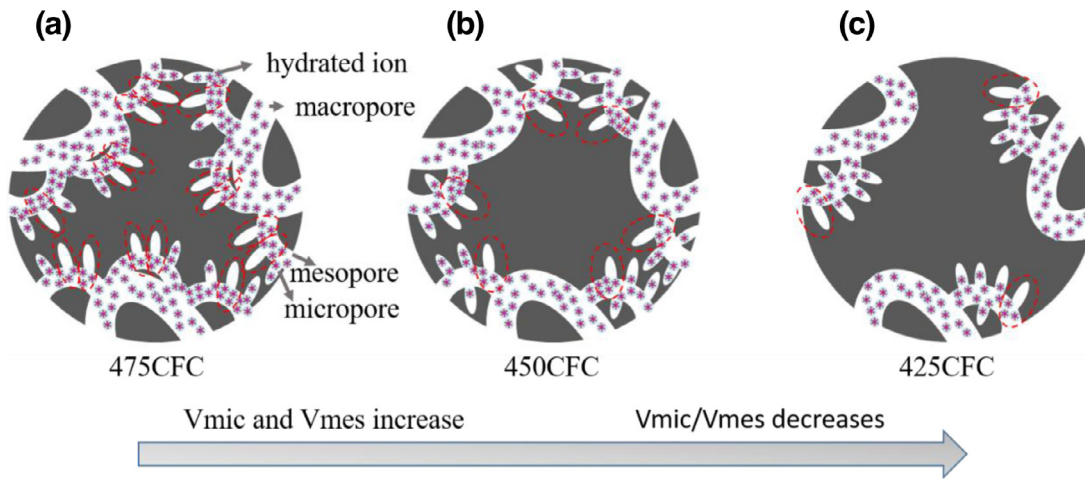
**Fig. 4.** Electrochemical characterizations. (a) CV curves of CFC, 425CFC, 450CFC and 475CFC at 5 mV/s. (b) GCD curves of the electrodes at 2 mA/cm<sup>2</sup>. (c) Current as a function of scan rate observed from narrow window CV curves collected using ACFCs electrodes. (d)  $N_2$  adsorption/desorption isotherms. (e) Differential pore volume distributions of CFCs at different temperatures and (f) the 2D-NLDFT model is used to calculate the pore size distribution.

**Table 1.** Different carbon materials are used as supercapacitor electrodes.

Samples	Capacitance (mF/cm <sup>2</sup> )	Current density	Potential window (V)	Reference electrode
nitrogen-doped CC [12]	322	2 mA/cm <sup>2</sup>	0–0.5	SCE
Activated carbon cloths [11]	88	10 mV/s	0–1	Ag/AgCl
thermally activated CC [8]	912	20 mA/cm <sup>2</sup>	0–1	Ag/AgCl
activated carbon cloths [10]	756	6 mA/cm <sup>2</sup>	0 to –1	SCE
treated carbon cloth [9]	2367	2.5 mA/cm <sup>2</sup>	0 to –1	SCE
NCNFs/CC [2]	608	1 mA/cm <sup>2</sup>	0 to –1	SCE
RGO/m-CC [4]	331	1 mA/cm <sup>2</sup>	0–1	Ag/AgCl
CFC-750-N-S [13]	362	0.5 mA/cm <sup>2</sup>	0–1	Hg/HgO
N-doped carbon cloth [1]	1200	8 mA/cm <sup>2</sup>	0 to –1	SEC
CQDs/PPy-50 [38]	516	10 mV/s	0.5 to –0.5	Ag/AgCl
MnO <sub>2</sub> /graphene [39]	500	5 mV/s	0–0.8	Hg/Hg <sub>2</sub> Cl <sub>2</sub>
MnO <sub>2</sub> @PANI@m-CC [40]	293.3	0.2 mA/cm <sup>2</sup>	0–0.8	SCE
MnO@C/CC [41]	716	4 mA/cm <sup>2</sup>	0.5 to –0.6	Hg/HgO
PANI/N-C/SS [42]	624	0.05 mA/cm <sup>2</sup>	0–0.8	Ag/AgCl
activated carbon fiber paper [43]	750	5 mA/cm <sup>2</sup>	0 to –0.9	SCE
This work	1324	2 mA/cm <sup>2</sup>	0 to –1	SCE

**Table 2.** The volumes of pores for CFC, 350CFC, 400CFC, 425CFC, 450CFC and 475CFC.

	< 2 nm ( $V_{\text{mic}}/V_t$ )	2~50 nm ( $V_{\text{mes}}/V_t$ )	> 50 nm ( $V_{\text{mac}}/V_t$ )	$V_{\text{mic}}:V_{\text{mes}}$
350CFC	0.03293(61.30%)	0.0194(36.11%)	0.00139(2.59%)	61.30: 36.11
400CFC	0.14247(84.04%)	0.02329(13.74%)	0.00377(2.22%)	84.04: 13.74
425CFC	0.14552(74.57%)	0.04768(24.43%)	0.00196(1%)	74.57: 24.43
450CFC	0.19873(70.22%)	0.08095(28.61%)	0.00331(1.17%)	70.22: 28.61
475CFC	0.26065(68.92%)	0.11575(30.61%)	0.00178(0.47%)	68.92: 30.61

**Fig. 5.** Schematic illustration of the relationship of hierarchical pores and electrolyte ions.

tance between the two layers ( $d$ ), which increases the capacitance abnormally. The 475CFC has the maximum  $V_{\text{mic}}$  and  $V_{\text{mes}}$  but the specific capacity is less than 450CFC. In fact, it is the coordination issue of  $V_{\text{mic}}$  and  $V_{\text{mes}}$  with electrolyte ions, from which we can propose a model, as shown in Fig. 5. When the CFCs are immersed in the electrolyte, the electrolyte ions first enter into the macropore for full contact with the electrode. Then the electrolyte ions further proceed into the mesoporous sites. The dense atomic layer on the adjacent pore wall provides the capacity in the relatively large mesopores. However, the capacitance decreases in relatively small mesopores because the impact of adjacent ion layers on the pore wall reduces the effective specific surface area [15]. The relationship between desorption average pore width and adsorption average pore width of 425CFC, 450CFC and 475CFC samples are 450CFC > 425CFC > 475CFC as shown in Fig. S4(b).

Subsequently, the ions in the mesopores further diffused into the micropores and even the ultra-micropores. Therefore, there may be congestion in the process of ion entering micropores because  $V_{\text{mic}}/V_{\text{mes}}$  is small in 475CFC (the red circles represent micropores where the congestion is likely to occur). So the micropores are not fully utilized as shown in Fig. 5(a). In 450CFC, the congestion is alleviated when  $V_{\text{mic}}/V_{\text{mes}}$  increases, the utilization of micropores is improved, as shown in Fig. 5(b). Compared with 425CFC, 450CFC and 475CFC, 425CFC has the largest  $V_{\text{mic}}/V_{\text{mes}}$ , as shown in Fig. 5(c); thus, the maximum utilization rate of micropores is achieved. Our hierarchical pores are analogue to a traffic system, the branches that link the main routes are crucial. Less branches and further forks cannot facilitate an effective ion transport. Macropores, mesoporous pores and micropores can be regarded as main routes, branches and forks, respectively. There is the maximum micropore utilization but less mesoporous in 425CFC. However, there are more mesopores in 475CFC, but the utilization of micropores is low. In 450CFC, an utilization of micropores and mesopores are balanced with affording more pore walls to form the double layer. So 450CFC with an appropriate hierarchical pores integration has the maximum specific capacity of 1324 mF/cm<sup>2</sup> at 2 mA/cm<sup>2</sup>. Therefore, hierarchical pores integra-

tion is crucial for the capacitance of CFC. In order to verify that CFC with such merits can provide more electrochemical active surface area (EASA), a narrow range of slow scanning speed was applied [33–35] (Fig. S5) and double-layer capacitance was acquired after fitting as Fig. 4(c). Herein the higher slope means higher EASA [36,37]. The slope of 425CFC, 450CFC and 475CFC is 0.47, 0.62 and 0.42, respectively. 450CFC has the largest EASA. The moderate hierarchical pores integration in 450CFC can provide more effective pore walls for the formation of double-layers.

Meanwhile, we also tested the rate performance. It gets worse with the increase of the content of micropores and mesopores during the annealing process as Fig. S6. The transport of electrolyte ions and electrons has an important influence on the rate stability in the process of fast charge and discharge. One model has indicated that the interaction between electrolyte ions and pore channels increases with the increase of pore depth. The resistance increases significantly when electrolyte ions enter the pores. These factors affect the rate stability of electrode materials [44]. Excessive micropores and mesopores are not conducive to fast charge and discharge. This is to say, the overall performance of CFC cannot be optimized by full expanding of micropores and mesopores. The electrochemical impedance spectroscopy (EIS) was used to further understand the charge transfer kinetics of these samples [45]. Figs. S7 and S8 and Table S2 is the electrode impedance diagram and the corresponding fitting information. 450CFC has the smallest equivalent series resistance ( $R_s$ ) and charge transfer resistance ( $R_{\text{ct}}$ ) compared with 425CFC and 475CFC. The smaller  $R_s$  represents the smaller resistance of active material and contact in 450CFC. The smaller  $R_{\text{ct}}$  represents the smaller charge transfer resistance and the improved ion transfer performance in the pores. This should be related to the integration of moderate hierarchical pores in 450CFC. Thus, comparing to the other two samples, our 450CFC affords the best capacitor performance. The cyclic stability is shown in Fig. S9. The capacitance maintenance of all the three materials decreased after 2000 charging-discharging test, whereas there is no significant difference between them. Meanwhile, large-scale 450CFC (12 × 4 cm<sup>2</sup>, judged from the color) was prepared as

shown in Fig. S10(a). The lower left was the original CFC. Then we randomly cut  $1 \times 1.5 \text{ cm}^2$  carbon fiber cloth (sample 1–450CFC, sample 2–450CFC, sample 3–450CFC) from the large size carbon fiber sheets for electrochemical testing as electrode materials, as Fig. S10(b). The specific capacity of sample 1–450CFC, sample 2–450CFC and sample 3–450CFC are 1240, 1340 and 1300 mF/cm<sup>2</sup>, respectively under the current density of 2 mA/cm<sup>2</sup>. The specific capacity of 450CFC is 1324 mF/cm<sup>2</sup>, which is very close to the specific capacity of the three samples. This result demonstrates that a relatively large sample can be uniformly activated.

#### 4. Conclusions

Carbon fiber cloths were treated by a simple one-step air annealing in order to obtain CFCs with an integration of different hierarchical pores. The activated CFCs directly used as the cathode in 1 M KOH aqueous solution for a supercapacitor, in which the maximum capacity of 450CFC sample reaches 1324 mF/cm<sup>2</sup> at the scanning rate of 2 mA/cm<sup>2</sup>. Such excellent performance is attributed to the combination of the optimal ratio of  $V_{\text{mic}}/V_{\text{mes}}$  in 450CFC and the appropriate mesoporous volumes. Our work further proves that the effect of  $V_{\text{mic}}/V_{\text{mes}}$ , rather than just increasing the mesoporous and microporous volumes, should be fully considered towards improving the CFC capacitance.

#### Declaration of Competing Interest

None.

#### Acknowledgments

This research is supported by the National Natural Science Foundation of China (51932003, 51872115, and 51802110), 2020 International Cooperation Project of the Department of Science and Technology of Jilin Province, Program for the Development of Science & Technology of Jilin Province (Item No. 20190201309JC), the Jilin Province/Jilin University co-Construction Project-Funds for New Materials (SXGJSF2017-3, Branch-2/440050316A36), the Open Project Program of Wuhan National Laboratory for Optoelectronics (2018WNLOKF022), the Program for JLU Science & Technology Innovative Research Team (JLUSTIRT, 2017TD-09), the Fundamental Research Funds for the Central Universities JLU, and “Double-First Class” Discipline for Materials Science & Engineering.

#### Supplementary materials

Supplementary material associated with this article can be found, in the online version, at doi:10.1016/j.jechem.2019.12.014.

#### References

- [1] Q. Zhang, N. Wang, P. Zhao, M. Yao, W. Hu, *J. Mater. Sci.* 53 (2018) 14573–14585.
- [2] Y.-N. Liu, J.-N. Zhang, H.-T. Wang, X.-H. Kang, S.-W. Bian, *Mater. Chem. Front.* 3 (2019) 25–31.
- [3] F.N.I. Sari, J.M. Ting, *ChemSusChem* 11 (2018) 897–906.
- [4] H. Jeon, J.M. Jeong, S.B. Hong, M. Yang, J. Park, D.H. Kim, S.Y. Hwang, B.G. Choi, *Electrochim. Acta* 280 (2018) 9–16.
- [5] W. Martin, R.J. Brodd, *J. Cheminform. Chem. Rev.* 35 (2004) 4245–4269.
- [6] Y. Huang, C. Zhi, *J. Phys. D: Appl. Phys.* 50 (2017) 273001.
- [7] P. Simon, Y.J.N.M. Gogotsi, *Nat. Mater.* 7 (2008) 845–854.
- [8] Q. Wang, W. Ren, F. Gao, C. Qiu, Q. Wang, F. Gao, C. Zhao, *ChemElectroChem* 6 (2019) 1768–1775.
- [9] H. Wang, J. Deng, C. Xu, Y. Chen, F. Xu, J. Wang, Y. Wang, *Energy Storage Mater.* 7 (2017) 216–221.
- [10] W. Wang, W. Liu, Y. Zeng, Y. Han, M. Yu, X. Lu, Y. Tong, *Adv. Mater.* 27 (2015) 3572–3578.
- [11] G. Wang, H. Wang, X. Lu, Y. Ling, M. Yu, T. Zhai, Y. Tong, Y. Li, *Adv. Mater.* 26 (2014) 2676–2682.
- [12] N.R. Chodankar, S.-H. Ji, D.-H. Kim, *J. Electrochem. Soc.* 165 (2018) A2446–A2450.
- [13] T. Ouyang, K. Cheng, F. Yang, J. Jiang, J. Yan, K. Zhu, K. Ye, G. Wang, L. Zhou, D.J.C.E. Cao, *Chem. Eng. J.* 335 (2017) 638–646.
- [14] W. Zhang, D. Wang, W. Zheng, *J. Energy Chem.* 41 (2020) 100–106.
- [15] J. Chmiola, G. Yushin, Y. Gogotsi, C. Portet, P. Simon, P.L. Taberna, *Science* 313 (2006) 1760–1763.
- [16] W.Y. Tsai, P.L. Taberna, P. Simon, *J. Am. Chem. Soc.* 136 (2014) 8722–8728.
- [17] K. Xia, Q. Gao, J. Jiang, J. Hu, *Carbon* 46 (2008) 1718–1726.
- [18] S.-W. Woo, K. Dokko, H. Nakano, K. Kanamura, *J. Mater. Chem.* 18 (2008) 1674–1680.
- [19] D.-W. Wang, F. Li, M. Liu, G.Q. Lu, H.-M. Cheng, *Angew. Chem.* 120 (2008) 379–382.
- [20] H.-J. Liu, J. Wang, C.-X. Wang, Y.-Y. Xia, *Adv. Energy Mater.* 1 (2011) 1101–1108.
- [21] Y. Gong, H. Wang, Z. Wei, L. Xie, Y. Wang, *ACS Sustain. Chem. Eng.* 2 (2014) 2435–2441.
- [22] H. Yang, X. Shi, T. Deng, T. Qin, L. Sui, M. Feng, H. Chen, W. Zhang, W. Zheng, *ChemElectroChem* 5 (2018) 3612–3618.
- [23] A. Zandiatashbar, G.H. Lee, S.J. An, S. Lee, N. Mathew, M. Terrones, T. Hayashi, C.R. Picu, J. Hone, N. Koratkar, *Nat. Commun.* 5 (2014) 4186.
- [24] L. Stobinski, B. Lesiak, A. Malolepszy, M. Mazurkiewicz, B. Mierzwa, J. Zemek, P. Jiricek, I. Bieloshapka, *J. Electron. Spectrosc.* 195 (2014) 145–154.
- [25] A.M. Puziy, O.I. Poddubnaya, R.P. Socha, J. Gurgul, M. Wisniewski, *Carbon* 46 (2008) 2113–2123.
- [26] S. Park, D.A. Dikin, S.T. Nguyen, R.S. Ruoff, *J. Phys. Chem. C* 113 (2009) 15801–15804.
- [27] J.-H. Zhou, Z.-J. Sui, J. Zhu, P. Li, C. De, Y.-C. Dai, W.-K. Yuan, *Carbon* 45 (2007) 785–796.
- [28] Y. Gong, D. Li, C. Luo, Q. Fu, C. Pan, *Green Chem.* 19 (2017) 4132–4140.
- [29] J. Jagiello, J.P. Olivier, *Carbon* 55 (2013) 70–80.
- [30] J. Jagiello, J. Kenvin, A. Celzard, V. Fierro, *Carbon* 144 (2019) 206–215.
- [31] K. Urita, N. Ide, K. Isobe, H. Furukawa, I. Moriguchi, *ACS Nano* 8 (2014) 3614–3619.
- [32] J. Dzubiella, J.P. Hansen, *J. Chem. Phys.* 122 (2005) 234706.
- [33] H. Shi, *Electrochim. Acta* 41 (1996) 1633–1639.
- [34] J. Kibsgaard, C. Tsai, K. Chan, J.D. Benck, J.K. Norskov, F. Abild-Pedersen, T.F. Jaramillo, *Energy Environ. Sci.* 8 (2015) 3022–3029.
- [35] K. Fan, H. Chen, Y.F. Ji, H. Huang, P.M. Claesson, Q. Daniel, B. Philippe, H. Rensmo, F.S. Li, Y. Luo, L.C. Sun, *Nat. Commun.* 7 (2016) 11981.
- [36] Y. Han, Y.Z. Lu, S.H. Shen, Y. Zhong, S. Liu, X.H. Xia, Y.X. Tong, X.H. Lu, *Adv. Funct. Mater.* 29 (2019) 1806329.
- [37] M. Carmo, T. Roepke, F. Scheiba, C. Roth, S. Moeller, H. Fuess, J.G.R. Poco, M. Linardi, *Mater. Res. Bull.* 44 (2009) 51–56.
- [38] X. Jian, H.-m. Yang, J.-g. Li, E.-h. Zhang, L.-l. Cao, Z.-h. Liang, *Electrochim. Acta* 228 (2017) 483–493.
- [39] Y. Zhang, Q. Zou, H.S. Hsu, S. Raina, Y. Xu, J.B. Kang, J. Chen, S. Deng, N. Xu, W.P. Kang, *ACS Appl. Mater. Inter.* 8 (2016) 7363–7369.
- [40] X. Zhao, C. Chen, Z. Huang, L. Jin, J. Zhang, Y. Li, L. Zhang, Q. Zhang, *RSC Adv.* 5 (2015) 66311–66317.
- [41] N. Yu, K. Guo, W. Zhang, X. Wang, M.-Q. Zhu, *J. Mater. Chem. A* 5 (2017) 804–813.
- [42] J. Cao, T. Huang, R. Liu, X. Xi, D. Wu, *Electrochim. Acta* 230 (2017) 265–270.
- [43] H. Zhang, W. Qiu, Y. Zhang, Y. Han, M. Yu, Z. Wang, X. Lu, Y. Tong, *J. Mater. Chem. A* 4 (2016) 18639–18645.
- [44] R.D. Levie, *Electrochim. Acta* 8 (1963) 751–780.
- [45] J. Liu, Y. Qiao, C.X. Guo, S. Lim, H. Song, C.M. Li, *Bioresour. Technol.* 114 (2012) 275–280.